

**Measurement of the Deeply Virtual Neutral Pion
Electroproduction Cross Section at the Thomas
Jefferson National Accelerator Facility at 10.6
GeV**

by

Robert Johnston

Submitted to the Department of Physics
in partial fulfillment of the requirements for the degree of

Interdisciplinary PhD in Physics and Statistics

at the

MASSACHUSETTS INSTITUTE OF TECHNOLOGY

August 2023

© Massachusetts Institute of Technology 2023. All rights reserved.

Author
.....

Department of Physics
August, 2023

Certified by
.....

Richard Milner
Professor of Physics
Thesis Supervisor

Accepted by
.....

Lindley Winslow
Associate Department Head of Physics

**Measurement of the Deeply Virtual Neutral Pion
Electroproduction Cross Section at the Thomas Jefferson
National Accelerator Facility at 10.6 GeV**

by

Robert Johnston

Submitted to the Department of Physics
on August, 2023, in partial fulfillment of the
requirements for the degree of
Interdisciplinary PhD in Physics and Statistics

Abstract

Deeply virtual exclusive reactions provide unique channels to study both transverse and longitudinal properties of the nucleon simultaneously, allowing for a 3D image of nucleon substructure. This presentation will discuss work towards extracting an absolute cross section for one such exclusive process, deeply virtual neutral pion production, using 10.6 GeV electron scattering data off a proton target from the CLAS12 experiment in Jefferson Lab Hall B . This measurement is important as exclusive meson production has unique access to the chiral odd GPDs, and is also a background for other exclusive processes such as DVCS, making the determination of this cross section crucial for other exclusive analyses.

Thesis Supervisor: Richard Milner
Title: Professor of Physics

Acknowledgments

To Be Completed.

Contents

List of Equations	9
1 Introduction	11
1.1 Exploring Structure through Scattering	13
1.1.1 Scattering at Different Resolution Scales	13
1.1.2 Elastic Scattering and Form Factors	15
1.1.3 Inelastic Scattering and Parton Distribution Functions	19
1.2 Process Background	27
1.2.1 Wigner Functions, Generalized Parton Distributions	27
1.2.2 Deeply Virtual Exclusive Processes	31
1.2.3 Status of DV π P Measurements	39
A Full Cross Section Data	53
B BSA Cross Check	55
C Derivation of phi math convention	57

List of Figures

1-1	J.J. Thomson's Plum Pudding Model	12
1-2	Elastic scattering diagram	15
1-3	Tree-level elastic scattering Feynman diagram	17
1-4	Fourier Transforms of Charge Distributions	19
1-5	Feynman Diagram for Inelastic Scattering	20
1-6	Scattering Cross Section vs. Energy Transfer	21
1-7	Proton Structure Function F_2^p	24
1-8	Parton Distribution Functions	25
1-9	Scattering Measurements at Different Scales	26
1-10	Relation cube, from (M. Burkardt and Pasquini, 2016).	30
1-11	DVCS and DVMP Feynman Diagrams	32
1-12	Proton Pressure Distribution from DVCS data, from (Burkert, Elouadrhiri, and Girod, 2018).	32
1-13	Proton Pressure Distribution from Lattice QCD, from (Shanahan and Detmold, 2019).	32
1-14	DVPiP Feynman Diagram	36
1-15	Diagram of Lepton-Hadron Plane angle ϕ	37
1-16	Kinematic Reach Comparison	41
1-17	Analysis Flowchart	43

B-1 BSA Cross Check Results	56
---------------------------------------	----

List of Tables

1.1 GPDs Across Nucleon and Quark Polarizations.	29
--	----

List of Equations

1.1	Diffraction Limit	14
1.2	de Broglie Relationship	14
1.3	Rutherford Scattering Differential Cross Section	16
1.4	Mott Scattering Differential Cross Section	16
1.5	Elastic Scattering Differential Cross Section	17
1.8	Rosenbluth Scattering Cross Section	18
1.9	Outgoing Hadronic System Invariant Mass W	20
1.10	Bjorken X	21
1.11	Inelasticity y	21
1.12	Energy Transfer ν	22
1.13	Lorentz-invariant Rosenbluth Scattering Cross Section	22
1.14	Scattering Cross Section in Terms of $F_1(x_B, Q^2)$ and $F_2(x_B, Q^2)$	22
1.15	F_2 structure function in terms of PDFs	23
1.16	Wigner Quasi-probability Distributions	28
1.17	Wigner Operator	28
1.18	Reduced Wigner Distribution	28
1.21	DV π P Cross Section Decomposition	38
1.22	Virtual Photon Flux	38

Chapter 1

Introduction

Humans have tried to understand the nature of the world around us for millennia, with discerning the structure of matter being a central effort in this quest. Famously, the Greek philosophers Leucippus and Democritus (\sim 5th century BCE) are credited with the concept of “atomism” - the belief that matter is composed of tiny indivisible particles called atoms (from the Greek $\alpha\tauομοσ$, roughly translating to “uncuttable” ([C.C.W. Taylor, 1999](#)). Even further back, there are Indian records from as early as the 8th century BCE conceptualizing the world as being built from tiny fundamental particles ([Thomas McEvilley, 2002](#)).

Scientific progress on this front stalled until the early 1800s, when chemists explored how different elements combined in to form compounds in specific, repeatable, small integer ratios. John Dalton formulated this idea as the Law of Multiple Proportions, which paved the way for early scientific atomic theory ([Britannica, 2010](#)). In 1897, J.J. Thomson discovered the first subatomic particle, the electron, by studying cathode rays([J. Thomson, 1901](#)). Accordingly, he devised a model of the atom which had electrons embedded in a ball of positively charged material, called the Thomson,

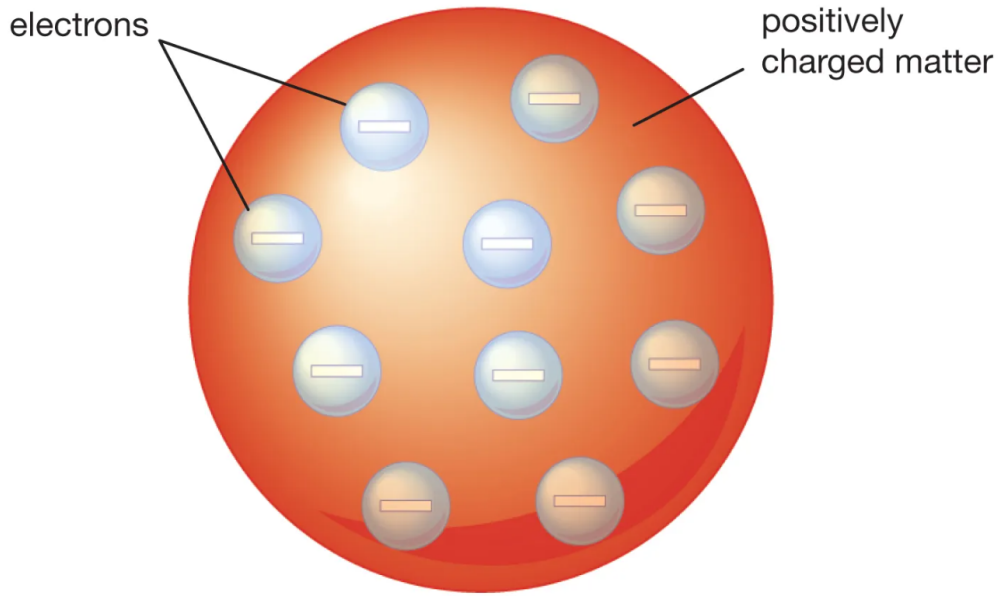


Figure 1-1: J.J. Thomson’s Plum Pudding Model of the atom ([Britannica, 2023](#))

or Plum Pudding, Model([Jaume Navarro, 1995](#)).

With the idea that the atom was a composite object, scientist began experimentation to study its exact structure. This was the start of what has been the 120 years of particle scattering studies to probe first atomic, then nuclear structure.

The rest of this chapter details the findings of previous scattering experiments and provides a background on Generalized Parton Distributions and Deeply Virtual Exclusive Processes, the topic of this work. Chapter 2 describes the experimental setup of the CLAS12 detector and data taking conditions. Chapter 3 discusses data analysis procedures to reconstruct particles and classify events from detector level information. Simulations and computational pipelines for this work are presented in chapter 4. The analysis procedure for combining experimental and simulated data into a differential cross section with correction factors is discussed in chapter 5.

Chapter 6 displays and discusses results and uncertainties. Chapter 7 summarizes this work and lays a path for finalizing the measurement. The appendices include numerous technical details and supplemental plots.

1.1 Exploring Structure through Scattering

The typical length scales for atoms and nucleons are 0.1 nm which is far smaller than the wavelength of human-visible light (~ 500 nm). As such, atomic and nuclear structure must be explored by forcing some interaction and then inferring the structure from the observed results. Thomson's atomic model was famously tested in the early 1900s by Ernest Rutherford's research group, wherein α particles were fired at thin metal targets, and the scattering behaviour was observed ([Geiger and Marsden, 1909](#)) ([Rutherford, 1911](#)).

The results were not consistent with Thomson's model, but instead indicated that there was a very small, dense, positively charged nucleus at the center of every atom. Further experiments by Rutherford would lead to the discovery of the proton around 1920 ([Rutherford, 1919](#)). Puzzles about the nucleus remained, including a consistent description of isotopes, until 12 years later when James Chadwick suggested the existence of the neutron ([Chadwick, 1932](#)). With electrons and the two nucleons discovered, it seemed as though the indivisible constituents of the atom were finally realized, but future experiments showed a much more complex, sub-nuclear structure.

1.1.1 Scattering at Different Resolution Scales

The diffraction limit for microscopic (compared to telescopic) systems can be approximated by equation 1.1, where n is the index of refraction, θ is a measure of the

device aperture, λ is the wavelength of the probe, and d is the minimum resolvable length scale. Thus, the wavelength of a probe sets a fundamental lower limit on the achievable resolution of a microscopic imaging system - roughly, at small enough distances, the probe's waves interfere, prohibiting resolution at or below that scale.

$$d = \frac{\lambda}{2n \sin \theta} \quad (1.1)$$

For visible light microscope systems, $\lambda \sim 500$ nm, and so the minimum resolvable feature size is approximately $d \sim 250$ nm. Techniques exist to extend the resolution size by approximately an order of magnitude, e.g. expansion microscopy ([Chen, Tillberg, and Boyden, 2015](#)) or Near-Field Scanning Optical Microscopy ([Ma et al., 2021](#)), but non-visible-light probes are needed for scales below ~ 10 nm.

In particular, the de Broglie relationship [1.2](#) ([Broglie, 1924](#)) states that the wavelength λ of a particle is inversely proportional to its momentum p , with h being Planck's constant.

$$\lambda = \frac{h}{p} \quad (1.2)$$

With this relationship, we can see that by increasing a particle's momentum, its effective wavelength is reduced. This is the fundamental principle which allows electron microscopes to image matter at a resolution of $\sim 10\text{-}0.1$ nm ([Franken et al., 2020](#)), corresponding to electron momenta of $\sim 1\text{-}100$ keV. At this scale, viruses, cells, molecular structures, and even atoms can be imaged ([Williams and Carter, 2009](#)), with striking results commonly published online. Other probes could be used to circumvent the diffraction limit, such as high energy (low-wavelength) photons or

high momentum (low de Broglie wavelength) protons or neutrons, but electrons are an ideal candidate in this regime as they are easy to produce, steer, interact with, and detect.

To move beyond imaging at the atomic scale ($\sim 1 \text{ \AA}$) to the nuclear scale ($\sim 1 \text{ fm}$) requires probes that are 100,000 times more powerful. Electrons are still an ideal probe due to their (apparent) lack of internal structure, but rather than a room sized microscope, an entire accelerator facility is needed to achieve high enough energies and luminosities for sub-nuclear scale resolution.

1.1.2 Elastic Scattering and Form Factors

Imaging with electrons (or other non-visible-light probes) at any energy scale is commonly understood in terms of scattering cross sections, σ , with dimensions of area and interpreted as the probability for a certain interaction to occur. Typical elastic scattering cross sections for transition metals with 100 keV incident electrons as in electron microscopy are $\sim 10^{-22} \text{ m}^2$ (Williams and Carter, 2009). In contrast, the cross sections to be discussed in this thesis are on the order of tens of nanobarn (10^{-36} m^2), or 14 orders of magnitude smaller.

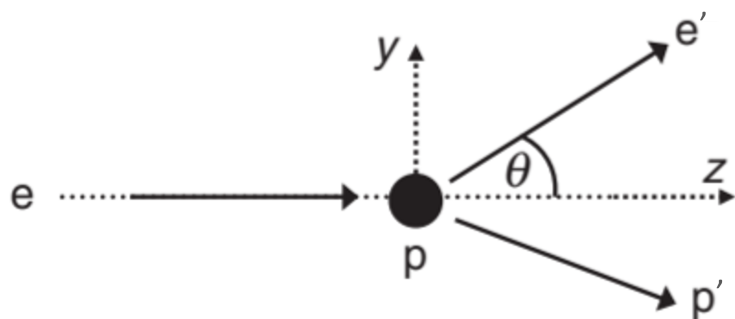


Figure 1-2: Elastic scattering diagram

The scattering cross section for a probe (such as an electron) incident on a target, can be calculated at lowest order by considering a fixed (no recoil), point-like (no structure), radially symmetric Coulomb potential (e.g., a proton) with a non-relativistic incident charged particle. The resulting equation was used by Rutherford's group in the discovery of the nucleus, and for an electron beam of energy E_{beam} is given by (1.3), where α is the fine structure constant.

$$\frac{\theta}{2} \left(\frac{d\sigma}{d\Omega} \right)_{Ruth} = \frac{\alpha^2}{16E_{beam}^2 \sin^4(\theta/2)} \quad (1.3)$$

To probe smaller resolution scales, it is necessary to increase the energy of the beam, and eventually the probe must be treated relativistically. This correction term is provided by the Mott scattering cross section, given by (1.4), which still assumes a fixed, point-like target, with only Coulomb interactions.

$$\left(\frac{d\sigma}{d\Omega} \right)_{Mott} = \frac{\alpha^2}{4E^2 \sin^4(\theta/2)} \cos^2 \frac{\theta}{2} = \left(\frac{\alpha}{2E \sin^2(\theta/2)} \cos \frac{\theta}{2} \right)^2 = 4 \cos^2 \frac{\theta}{2} \left(\frac{d\sigma}{d\Omega} \right)_{Ruth} \quad (1.4)$$

At higher incident electron energies (and thus finer spatial resolutions), the proton's finite size must be accounted for, as well as the momentum transferred to it. The tree-level Feynman diagram for elastic electron-proton scattering is show in Fig. 1.1.2. The incoming electron e exchanges a virtual photon with the proton p , resulting in a momentum transfer of $q = p_{e'} - p_e$.

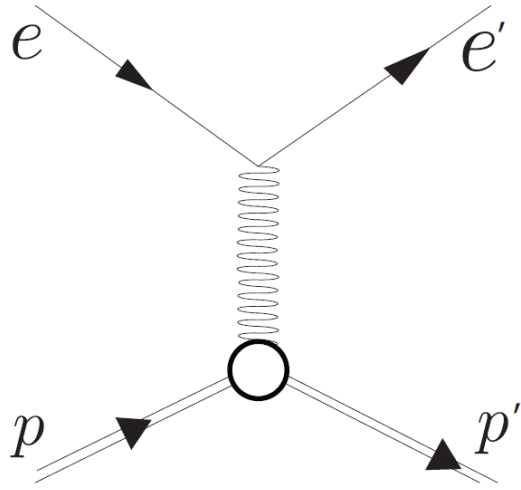


Figure 1-3: Tree-level elastic scattering Feynman diagram

The momentum transfer q sets the resolution scale for these processes, but it is convenient to work with the negative square of this value, defined as $Q^2 = -q^2$. With this term, we can express the relativistic differential cross section for the scattering of electrons off a resting, point-like proton as in (1.5), where m_p is the mass of the proton.

$$\frac{d\sigma}{d\Omega} = \frac{\alpha^2}{4E_{beam}^2 \sin^4(\theta/2)} \frac{E_{e'}}{E_{beam}} \left(\cos^2 \frac{\theta}{2} + \frac{Q^2}{2m_p^2} \sin^2 \frac{\theta}{2} \right) \quad (1.5)$$

Compared with Mott Scattering, there are two differences in this formula: The $\frac{E_{e'}}{E_{beam}}$ term in the scattering cross section comes from the electron losing energy to the proton's final state kinetic energy (no longer fixed), and the term proportional to $\sin^2(\theta/2)$ is due to a purely magnetic spin-spin interaction.

If the proton were a point, then (1.5) would agree with experiment for all electron

scattering energies. Instead, deviations are observed as we increase the beam energy. To account for this structure, we need to include two form factors, $G_E(Q^2)$ - related to the distribution of charge, and $G_M(Q^2)$, related to the distribution of magnetism inside the proton. In the low- Q^2 limit, these form factors are the Fourier transforms of the charge and magnetic moment distributions as in (1.6) and 1.7, reducing to the charge and the magnetic moment of the proton in the $Q^2 = 0$ limit.

$$G_E(Q^2) \approx G_E(q^2) = \int e^{iq \cdot r} \rho(r) d^3r \quad G_E(0) = \int \rho(r) d^3r = 1 \quad (1.6)$$

$$G_M(Q^2) \approx G_M(q^2) = \int e^{iq \cdot r} \mu(r) d^3r \quad G_M(0) = \int \mu(r) d^3r = 2.79 \quad (1.7)$$

Including these form factors in our cross section gives us the full elastic scattering cross section, as shown in (1.8).

$$\frac{d\sigma}{d\Omega} = \frac{\alpha^2}{4E_1^2 \sin^4(\theta/2)} \frac{E_3}{E_1} \left(\frac{G_E^2 + \tau G_M^2}{1 + \tau} \cos^2 \frac{\theta}{2} + 2\tau G_M^2 \frac{Q^2}{2m_p^2} \sin^2(\frac{\theta}{2}) \right) \quad (1.8)$$

Where $\tau = \frac{Q^2}{4m_p^2}$.

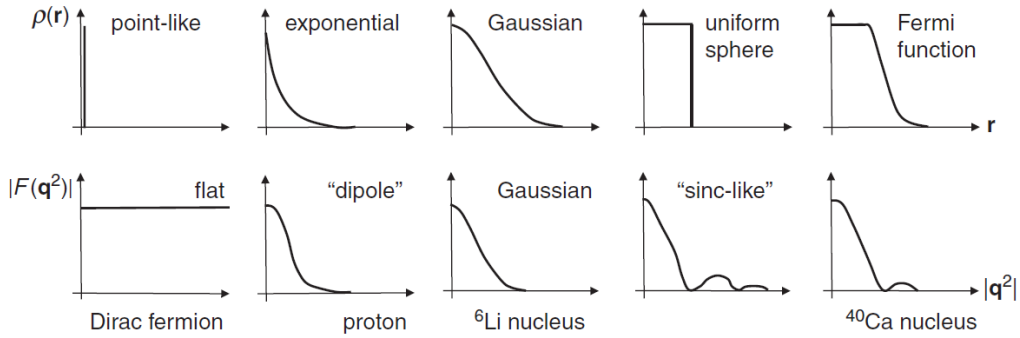


Figure 1-4: Samples of charge distributions and their corresponding form factors $F(\mathbf{q}^2)$, from ([M. Thomson, 2013](#))

By the 1960s, elastic scattering had been studied sufficiently well as to measure the proton form factors up to several GeV in Q^2 . The observed results were consistent with a proton having a ‘dipole’ form factor, as shown in Fig. 1.1.2. Investigating proton structure at finer spatial resolutions requires increasing the beam energy, but eventually the the elastic scattering cross section becomes negligible and instead the interactions are sufficiently energetic so as to create additional particles.

1.1.3 Inelastic Scattering and Parton Distribution Functions

Elastic scattering can be defined as interactions where the target stays intact; specifically, the variable W is the invariant mass of the outgoing struck target (1.9), where elastic scattering satisfies the condition $W^2 = m_p^2$. If $W^2 > m_p^2$, we instead have inelastic scattering, written as $e p \rightarrow e' X$, where X stands for some outgoing hadronic system, as shown in the Feynman diagram in Fig. 1-5.

$$W^2 \equiv (p_p + q)^2 = (p_p + (p_e - p_{e'}))^2 \quad (1.9)$$

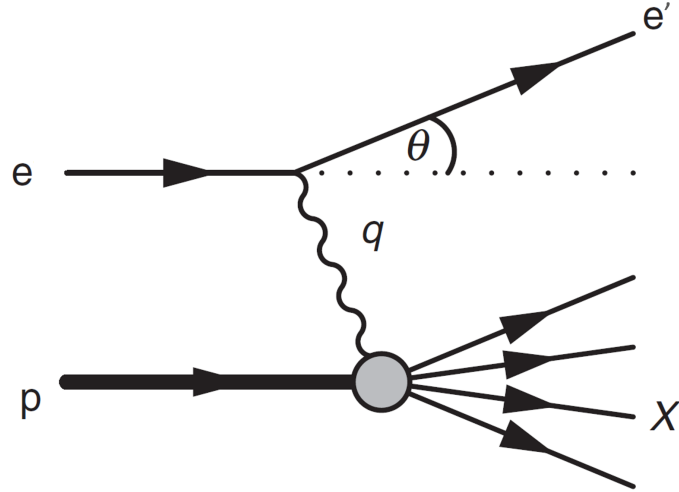


Figure 1-5: Feynman Diagram for Inelastic Scattering

The cross section for inelastic scattering has several peaks at various proton resonances, as indicated in the top sketch of Fig. 1-6. Continuing to higher energy transfers we reach the ‘Deep Inelastic Scattering’ (DIS) regime, defined by kinematics as $Q^2 > 1 \text{ GeV}^2$ and $W^2 > 4 \text{ GeV}^2$. Note that in the DIS process, the proton is smashed apart, yielding many subparticles. Other high-energy inelastic processes where the proton is left intact will be discussed in section 1.2.1.

Since we remove the constraint that the mass of the final state is the proton mass, we now have one extra degree of freedom, i.e., we need at least 2 variables to describe scattering here. Convenient choices are the squared four-momentum transfer of the virtual photon Q^2 and Bjorken X , defined in (1.10). x_B is a measure of elasticity: $x_B = 1$ for elastic scattering. It is useful in that it can also be interpreted as the fraction of proton momentum carried by the struck quark in the infinite momentum frame.

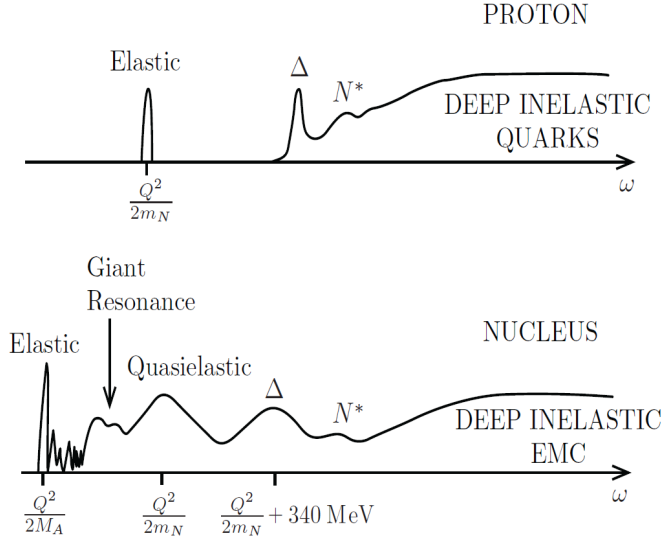


Figure 1-6: Sketch of cross section as a function of electron energy transfer for inclusive electron scattering off a proton (top) and a nucleus (bottom), from ([T. W. Donnelly et al., 2017](#))

$$x_B \equiv \frac{Q^2}{2p_p \cdot q} = \frac{Q^2}{Q^2 + W^2 - m_p^2} \quad (1.10)$$

Another useful quantity is y , which is a measure of the inelasticity of the scattering. It is the fractional energy lost by the electron in the scattering process, where $y=0$ is for perfectly elastic collisions, and is given by (1.11)

$$y \equiv \frac{p_p \cdot q}{p_p \cdot p_e} = \frac{\nu}{E_{beam}} = 1 - \frac{E_{e'}}{E_{beam}} \quad (1.11)$$

Where ν is the energy transferred in the collision (1.12).

$$\nu = \frac{Q^2}{2 * x_B * m_p} \quad (1.12)$$

With these definitions, we can write the differential cross section for inelastic scattering. Note that the general formula for the differential cross section for elastic scattering, (1.8) can be re-written in explicitly Lorentz-invariant form as in (1.13).

$$\frac{d\sigma}{d\Omega} = \frac{4\pi\alpha^2}{Q^4} \left[\left(1 - y - \frac{m_p^2 y^2}{Q^2}\right) \frac{G_E^2 + \tau G_M^2}{1 + \tau} + y^2 \frac{G_M^2}{2} \right] \quad (1.13)$$

This equation can be generalized to extend to inelastic scattering by replacing the terms corresponding to the combinations of form factors G_E and G_M with more structure functions $F_1(x_B, Q^2)$ and $F_2(x_B, Q^2)$, which describe proton structure as a function of both independent variables. This results in the differential cross section given by (1.14) .

$$\frac{d\sigma}{d\Omega} = \frac{4\pi\alpha^2}{Q^4} \left[\left(1 - y - \frac{m_p^2 y^2}{Q^2}\right) \frac{F_2(x_B, Q^2)}{x_B} + y^2 F_1(x_B, Q^2) \right] \quad (1.14)$$

Experiments in the 1960s on DIS indicated that the structure functions $F_1(x_B, Q^2)$ and $F_2(x_B, Q^2)$ were nearly independent of Q^2 , a feature known as Bjorken scaling (Bjorken and Paschos, 1969). This indicated scattering was occurring off of point-like constituents - current experiment results provide a constraint on the maximum radius of these constituent to be at most 10–18 m (M. Thomson, 2013).

Secondly, DIS results indicated the two structure functions could be expressed as

$F_2(x_B) = 2 * x_B * F_1(x_B)$, named the Callan-Gross relation. This relationship can be explained if the electron is scattering off of spin-half point-like particles inside the proton, which combined with Bjorken scaling to give strong evidence for the existence of quarks inside the proton, and gave motivation for the development of the parton model (Feynman, 1969). The parton model connects the experimentally measurable structure functions to Parton Distribution functions which describe the distribution of proton longitudinal momentum amongst its constituents. Specifically, a PDF $q_i(x_B)$ describes the probability density of finding a parton carrying a longitudinal momentum fraction in the interval $(x_B, x_B + dx_B)$. The relationship between PDFs and structure functions is given by (1.15), where Q_i is the charge of each quark.

$$F_2^p(x_B) = x_B \sum_i Q_i^2 q_i(x_B) \quad (1.15)$$

Structure functions have been studied in great detail over a very large kinematic range across Q^2 and x_B , the results of which are shown in Fig. 1-7.

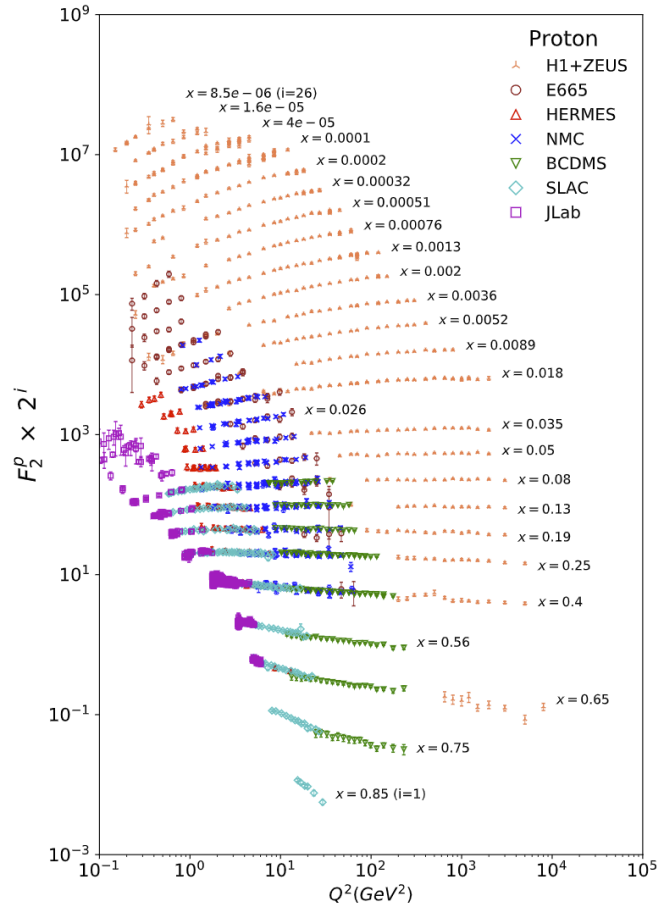


Figure 1-7: The proton structure function F_2^p , measured at various experiments as listed, all with $W^2 > 3.5\text{GeV}^2$. F_2^p values have been multiplied by 2^{ix} for visual purposes, from ([Zyla et al., 2020](#))

The global experimental results can be combined with theoretical QCD frameworks such as the DGLAP evolution equations ([Altarelli and Parisi, 1977](#)). to plot PDFs for various constituents of the proton, as shown in Fig. 1-8.

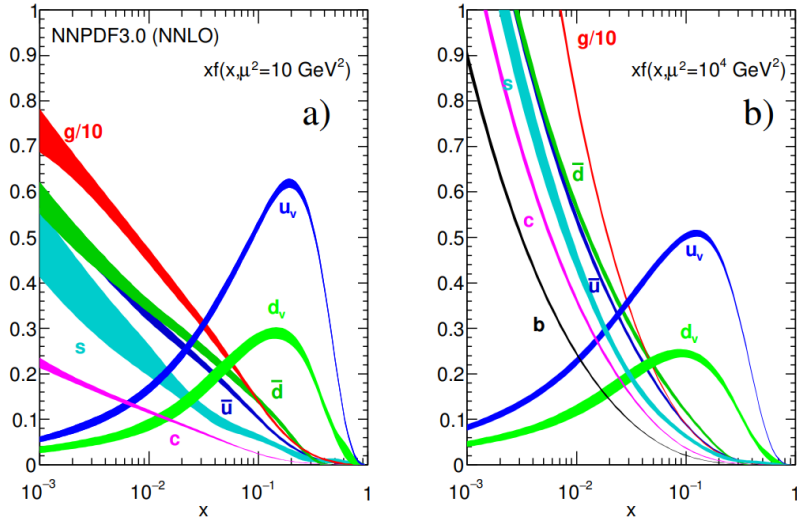


Figure 1-8: Quark and gluon distribution functions from NNLO NNPDF3.0 global analysis at $\mu^2 = 10 \text{ GeV}^2$ (left) and $\mu^2 = 10^4 \text{ GeV}^2$ (right), from (Zyla et al., 2020)

All of these major scattering scales explored through the 20th century are summarized in Fig. 1-9, spanning roughly four orders of magnitude in length scale. While steady increases in resolving power have been made, the focus of this work (red triangle in figure) is not to image even finer scale parton dynamics, but rather to understand the multidimensional structure of the nucleon. In particular, while PDFs allow for a 1 dimensional mapping of the inner workings of a proton, even more information can be gleaned from more complex scattering reactions. Efforts are now directed towards so called *proton tomography* - 3D imaging of nucleon structure - which is the focus of this analysis.

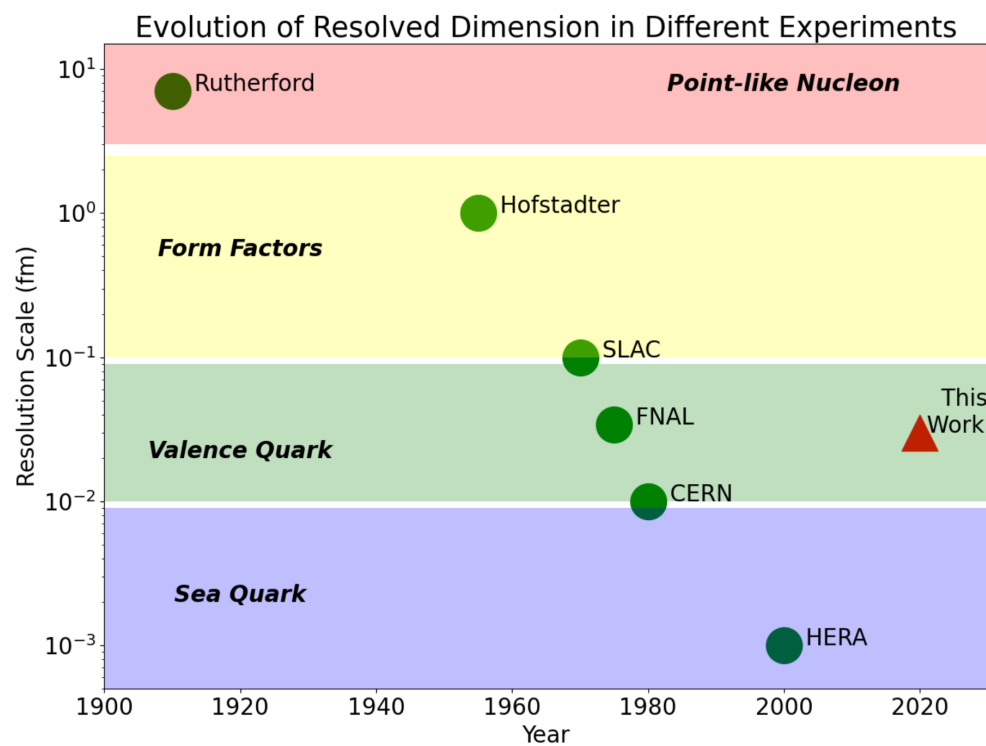


Figure 1-9: Scattering experiments performed at different energy scales reveal different information about proton structure. This work (red triangle) focuses on multi-dimensional structure mapping in the valence quark regime. Figure modified from ([Klein, 2005](#))

1.2 Process Background

The term *tomography* is derived from the Greek word *tomos*, which translates to *slice* or *section*. In the medical field, CT scans (computed tomography) combine many 2-D images from X-ray scans to generate a three-dimensional reconstruction of bodily organs. Building on this, proton tomography harnesses many nuclear reactions to reconstruct multi-dimensional mappings of partons' spatial and momentum distributions inside nucleons.

1.2.1 Wigner Functions, Generalized Parton Distributions

In classical mechanics, a particle can be completely described by its position in its six-dimensional phase space (three spatial and three momentum coordinates). An ensemble of such particles can be most completely understood through its phase space distribution function, which contains the probability of finding a particle in a particular region in phase space. In quantum systems, a pure phase space distribution is not well defined because of Heisenberg's uncertainty principle. However, in 1932 Eugene Wigner introduced a formalism that addressed this ([Wigner, 1932](#)), yielding functions provide the most comprehensive representation achievable for quantum systems.

Wigner Quasi-probability Distributions

Wigner Quasi-probability Distributions, commonly referred to as simply Wigner functions or Wigner distributions, are defined as in [\(1.16\)](#). This can be integrated over x (p) to yield momentum (space) density, but for arbitrary (x,p) the distribution can take negative values, and so violates probability axioms and thus is a quasi-probability distribution rather than a full probability distribution. Wigner

distributions are useful outside of particle physics, notably in signal processing, with more details available in (Hillery et al., 1984).

$$W(x, p) = \frac{1}{\pi\hbar} \int_{-\infty}^{\infty} \psi^*(x + \eta)\psi(x - \eta)e^{2ip\eta/\hbar}d\eta \quad (1.16)$$

The corresponding generalization to relativistic quark and gluon phase space distributions is covered in (Ji, 2004) to yield a Wigner Operator (1.17) which can be used to obtain the reduced quantum phase-space quark distributions in the nucleon (1.18).

$$\hat{W}_{\Gamma}(\vec{r}, k) = \int_{-\infty}^{\infty} e^{ik\cdot\eta} \bar{\Psi}(\vec{r} - \eta/2) \Gamma \Psi(\vec{r} - \eta/2) d^4\eta \quad (1.17)$$

$$W_{\Gamma}(\vec{r}, \vec{k}) = \int \frac{dk^-}{4\pi^2} \frac{1}{2} \int \frac{d^3\vec{q}}{8\pi^3} e^{-i\vec{q}\cdot\vec{r}} \langle \vec{q}/2 | \hat{W}_{\Gamma}(\vec{r}, k) | -\vec{q}/2 \rangle \quad (1.18)$$

Here we have integrated over $k^- = (k^0 - k^z)/\sqrt{2}$, the light-cone energy, since it is difficult to measure in high-energy processes.

Generalized Parton Distributions

No known experiments currently exist that are able to directly measure this distribution (nor is it known if it is possible). Fortunately, in recent decades theorists have been able to link experimental observables to further reduced forms of (1.18). Specifically, integration can be performed over spatial coordinates to yield Transverse Momentum Distributions (TMDs) which are outside the scope of this work.

Alternatively, integration can be performed over momentum coordinates to yield Generalized Parton Distributions (GPDs), which encode transverse spatial as well as longitudinal momentum distributions of partons inside the nucleon. As shown in ([Ji, 2004](#)), at leading-twist (twist-2), iterating through all choices of the Dirac matrix for quark distributions Γ yields 8 distinct GPDs. They are generally expressed in terms of parton momentum fraction x , skewness $\xi = \frac{-q^2}{q \cdot P} \sim \frac{x_B}{2-x_B}$, and momentum transfer t .

4 correspond to helicity conserving (chiral even) processes and 4 correspond to helicity flipping (chiral odd) processes: H , E , \tilde{H} , and \tilde{E} for chiral even, and H_T , E_T , \tilde{H}_T , and \tilde{E}_T ($\tilde{E}_T = 2^*\tilde{H}_T + E_T$ is commonly used). Table 1.2.1 summarizes the GPDs with respect to polarization states.

Nucleon		Quark Polarization		
Polarization		U	L	T
U	H	*	$\tilde{E}_T = 2^*\tilde{H}_T + E_T$	
L	*	\tilde{H}		$\tilde{E}_T?$
T	E	$\tilde{E}?$		H_T, \tilde{H}_T

Table 1.1: GPDs Across Nucleon and Quark Polarizations. * forbidden by parity.

GPDs can be understood by considering further integrations and forward limits - in the same way that the nucleon charge must be recovered when integrating over PDFs or Form Factors, these functions themselves are recovered when appropriately integrating over GPDs, as in Fig. 1-10. Specifically, first moments of the GPDs H and E are related to the Dirac and Pauli form factors F_1 and F_2 respectively:

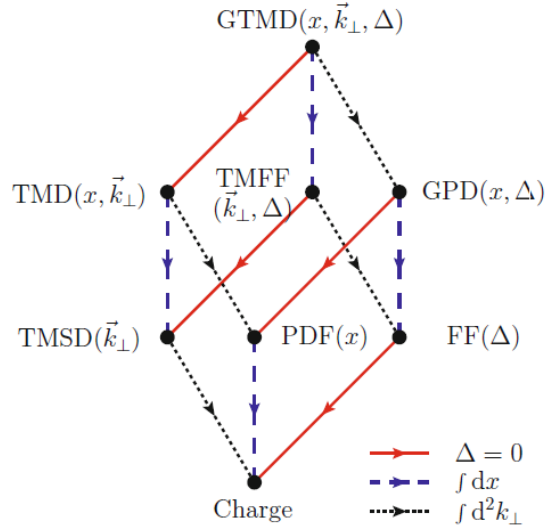


Figure 1-10: Relation cube, from (M. Burkardt and Pasquini, 2016).

$$\int dx H(x, \xi, t) = F_1(t) \quad (1.19)$$

$$\int dx E(x, \xi, t) = F_2(t) \quad (1.20)$$

Ji discusses gauge-invariant spin in his 1997 study (Ji, 1997). attempt to understand pion production (Goloskokov and Kroll, 2010) Burkardt's 2007 work investigates Generalized Parton Distributions (GPDs) (Matthias Burkardt, 2007).

In addition to collinear momentum distribution of partons inside the nucleon, GPDs also encode the distribution of partons in the plane transverse to the nucleons momentum in the infinite momentum frame [58]. Moreover, their relation to energy-momentum tensor (EMT) form factors allow us to access the EMT densities, the distribution of energy, angular momentum, pressure, and shear forces inside the

nucleon

1.2.2 Deeply Virtual Exclusive Processes

GPDs were realized to be experimentally accessible CITE through deeply virtual exclusive processes (DVEP) through factorization theoremss, involving the scattering of a virtual photon off a nucleon target, yielding either a real photon or mesons, along with an intact final state nucleon and incident particle (e.g. from an electron or muon beam). These processes are in stark contrast to DIS, where the nucleon target is shattered into many pieces, and can instead be thought of as a hard yet precise peaceful process.

deeply virtual π^0 (as well as η, η') production off a proton target is clearly distinct from the other types of meson production processes in that it involves the transition of a (virtual) photon with $JPC = 1-$ to a $JPC = 0+$ state (i.e. the final π^0 or η, η') requiring odd C-parity and chiral odd t-channel quantum numbers For example, the phi, on which F-X and Patrick are working, is very sensitive to the gluon distribution in the nucleon. therefore DVCS is primarily sensitive to non-quark spin flip - eg. H.. The same is true with DVMP of other vector meson, such as rho. However, since the pi0 and eta are $JP=0-$, then the transverse photon part contributing to the overall reaction cross section can cause a transversely polarized quark helicity flip. This is contained mainly in the structure functions σT and $\sigma T T$, which can be decomposed into the transversity GPDs - mainly EbarT and HT

Deeply Virtual Compton Scattering and Meson Production

Fig. 1-11 illustrates diagrams for Deeply Virtual Compton Scattering (DVCS) and Deeply Virtual Meson Production (DVMP).

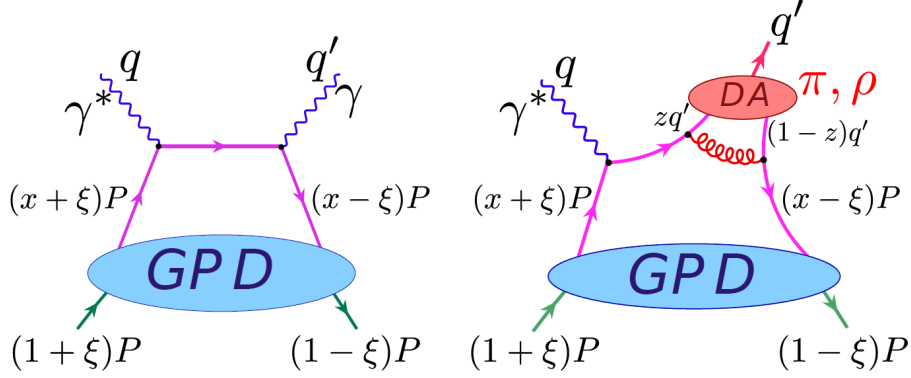


Figure 1-11: Feynman diagrams for DVCS (left) and DVMP (right), from (Kubarovsky, 2011). DA refers to the appropriate meson distribution amplitude.

DVCS is widely regarded as the “cleanest” channel and has already been leveraged to provide great insights into the structure of the nucleon. For example, Fig. 1-12 shows the pressure distribution inside a proton from DVCS data (Burkert, Elouadrhiri, and Girod, 2018), which has since been further investigated by theorists to generate similar mappings through LQCD as in Fig. 1-13

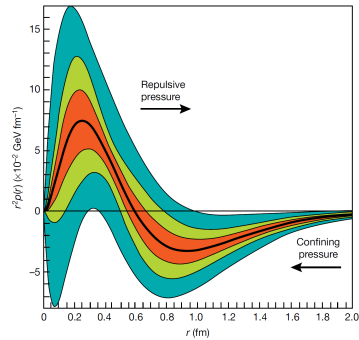


Figure 1-12: Proton Pressure Distribution from DVCS data, from (Burkert, Elouadrhiri, and Girod, 2018).

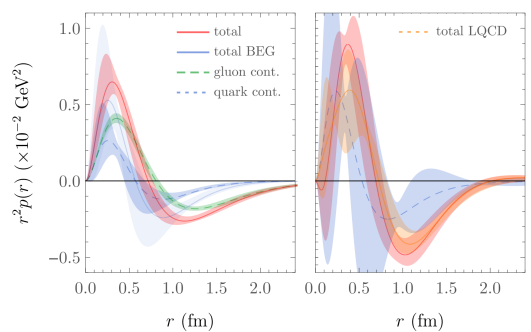


Figure 1-13: Proton Pressure Distribution from Lattice QCD, from (Shanahan and Detmold, 2019).

By measuring DVMP, we can get information about GPDs in the following way: in the leading twist approximation / some other formalism bullshit, dvmp cross section is described by the generalized Compton form factors, which themselves are (to leading twist etc.) convolutions of GPDs, so the dvmp cross section sets constraints on GPD behavior. Hard exclusive pseudoscalar meson electroproduction in recent years has shown that the asymptotic leading twist approximation is not readily applicable in the range of kinematics accessible to current experiments. In fact, there are strong contributions from transversely polarized virtual photons that are asymptotically suppressed by $1/\alpha^w$ in the cross sections and have to be considered by introducing chiral-odd GPDs into the framework.

So $Q^2 > 1$ is indeed for deeply virtual events, however it has no relation with lepton/hadron angle. There are π^0 events in the region below 1GeV^2 , and they are also π^0 events. The limit on 1GeV^2 is somewhat artificial. Ideally we are looking at the asymptotic freedom, so Q^2 should be infinity, but we are hoping that 1GeV^2 is big enough to apply models that are based on asymptotic freedom. There are many terms also that are proportional to powers of t/Q^2 . So we need reasonably big Q^2 to apply GPDs models. And in fact CLAS kinematics is often questioned to be too small for GPDs theoretical models.

DVMP is sensitive to chiral odd GPDs, distinguishing it from DVCS as a GDP probe because why? Because something involving photon helicity and pion helicity, I forget exactly though

In DVCS the incident and outgoing particles are both photons $JP = 1^-$. Therefore, no quark helicity flip is necessary in this “virtual Compton scattering”. Therefore DVCS is primarily sensitive to non-quark spin flip - eg. H.. The same is true with DVMP of other vector meson, such as rho.

First, note that not all DVMP reactions are sensitive to nuclear transversity dis-

tributions, which involves quark helicity flip of transversely polarized quarks helicity. This can occur in production of pseudoscalar mesons, e.g. pi0 and eta production, with spin-charge-parity I-PC= 0 - + ,in contrast with the incident photon, which has J-P 1- -.

This is not the case for other mesons studied at JLab, such as vector mesons, I-PC= 0 - e.g. the rho, omega, phi, for which which I-CP= 1- -, the same as for the photons.

I believe this was first pointed out Ahmad, Goldstein, Liutti (arXiv:0805.3568).

Here is a quote from their intro. "... deeply virtual π^0 (as well as η, η') production off a proton target is clearly distinct from the other types of meson production processes in that it involves the transition of a (virtual) photon with JPC = 1- to a JPC = 0+ state (i.e. the final π^0 or η, η') requiring odd C-parity and chiral odd t-channel quantum numbers. As a consequence, in a partonic description such as the one depicted in Fig.1a, the "outgoing" and "returning" quark helicities need to be opposite to one another . . .".

By the way, the other meson production channels are uniquely sensitive to other interesting aspects of nucleon structure. For example, the phi, on which F-X and Patrick are working, is very sensitive to the gluon distribution in the nucleon.

However, since the pi0 and eta are JP=0-, then the transverse photon part contributing to the overall reaction cross section can cause a transversely polarized quark helicity flip. This is contained mainly in the structure functions σ_T and σ_{TT} , which can be decomposed into the transversity GPDs - mainly $Ebar_T$ and H_T .

Also, pion and eta production can still also be accompanied by non-quark helicity flips, which would be mainly contained in the longitudinal structure functions σ_{LL} . However, various theoretical papers indicate that in our accessible region of Q^2 , σ_T and σ_{TT} dominate relative to σ_L . Experimentally, this seems to be verified from JLab

data . On the other hand, theory predicts that asymptotically, σ_L will dominate. From our existing 5 GeV data, we are not anywhere near there, so our experiments at JLab are really just right for accessing these transversity distributions. But, to decompose these distributions at the level of the individual quark u d flavors, we need as much precision data over as big a range as possible of kinematics in several channels - P-pi0, N-pi0, P-eta, N-eta. And, only you guys can do that! So, let me know if this makes sense to you. s a bit.

Why is Phi particularly sensitive to the phi distribution?

If you look at the proposal you will see the main diagram we are interested in has a pair of gluons from the GPD bag connecting a the hard scattering kernel that comes from the virtual photon fluctuating into a $s\bar{s}$ pair

The process you mention instead has a pair of strange quarks from the GPD bag connecting to the hard scattering kernel directly.

In practice the two processes happen. From known PDF however the gluon contribution is expected to be significantly larger than the strange quarks contribution. So the intuitive reason would be: the proton has nearly no strangeness but does have a bunch of gluons.

Now it could be that we are wrong and that the proton has more strangeness than what conventional PDF suggest. This could potentially hamper our strategy. However, intrinsic strangeness is in itself a very interesting subject, and if we did come to the conclusion that the proton has more strangeness than is conventionally accepted, then it would be a very important result.

The way I understand why the phi channel probes the gluon GPDs is because the phi meson is a strange-antistrange meson, and so doesn't interact with the up and down quarks that predominantly make up the quark content of the nucleons. This is from the phi cross section proposal: Because of its almost pure $s\bar{s}$ composition

ϕ production is not affected by scattering from the nucleon's valence quarks or the light quark sea;

also ([Diehl et al., 2020](#)) test ([Matthias Burkardt, 2007](#))

Deeply Virtual Neutral Pion Production

Only valence quarks contribute electroproduction of uncharged pions.

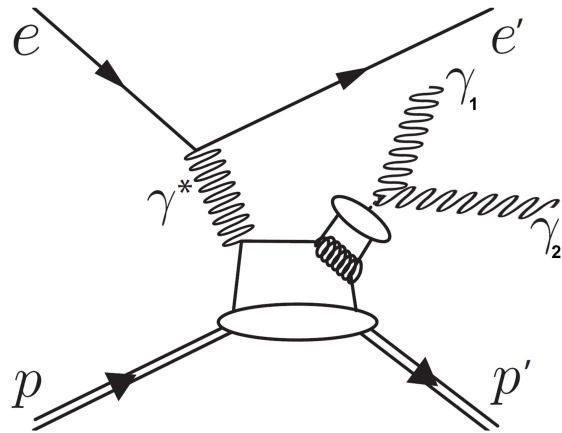


Figure 1-14: DV π^0 P Feynman Diagram

The cross-section for DV π^0 P ([1.21](#)) can be theoretically linked in terms of structure functions to GPDs by [mechanism of linking](#), which describe the 3D structure of the nucleon.

Several weeks ago I remarked in our meeting that I was having difficulty finding an explanation for the specific form of the DVMP cross section written in terms of structure functions (example below). Papers normally state that the relation holds without justification. I tried to follow the papertrail for the origin but so far have not ultimately been successful. Igor has kindly found a paper from 1992 (Dreschsel and Tiator pdf ([iop.org](#)) which makes reference (page 460, eq 18 - 19) ([Dreschsel and](#)

Tiator, 1992) (Bedlinskiy et al., 2014) to Donnachie and Shaw (Generalized Vector Dominance 1978) (Donnachie and Shaw, 1978)

In the attached, Bill Donnelly and colleagues have recently published a long paper on the general tensor structure for electron scattering in terms of invariant responses. In Eq (46), they derive a general expression for the Lorentz invariant part of the spin (T. Donnelly, Jeschonnek, and Van Orden, 2023) dependent cross section. The unpolarized piece has the identical L/T/TT/TL form you have. I have not read the paper in detail but I think you may find it useful.

Origin of form and interpretation of virtual photon flux gamma: (Amaldi, Fubini, and Furlan, 1979) page 6

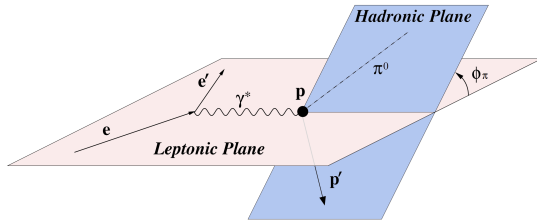


Figure 1-15: Diagram of Lepton-Hadron Plane angle ϕ

$$\frac{d^4\sigma_{ep \rightarrow ep' \pi^0}}{dQ^2 dx_B dt d\phi_\pi} = \Gamma(Q^2, x_B, E) \frac{1}{2\pi} \left\{ \left(\frac{d\sigma_T}{dt} + \epsilon \frac{d\sigma_L}{dt} \right) + \epsilon \cos(2\phi) \frac{d\sigma_{TT}}{dt} + \sqrt{2\epsilon(1+\epsilon)} \cos(\phi) \frac{d\sigma_{LT}}{dt} \right\} \quad (1.21)$$

Here Γ is the virtual photon flux as in (1.22), ϵ is the virtual photon polarization (1.23), and the structure functions can be expressed as convolutions of GPDs as shown in (1.24)-(1.27)

From (Amaldi, Fubini, and Furlan, 1979), Gamma is of electromagnetic origin and contains the effect of the electron-photon vertex and the photon propagator. It can be interpreted as the number of virtual photons per scattered electron

Epsilon can be interpreted as the ratio of transverse to longitudinally polarized photons

$$\Gamma(Q^2, x_B, E) = \frac{\alpha}{8\pi} \frac{Q^2}{m_p^2 E^2} \frac{1 - x_B}{x_B^3} \frac{1}{1 - \epsilon} \quad (1.22)$$

$$\epsilon = \frac{1 - y - \frac{Q^2}{4E^2}}{1 - y + \frac{y^2}{2} + \frac{Q^2}{4E^2}} \quad (1.23)$$

$$\frac{d\sigma_L}{dt} = \frac{4\pi\alpha}{kQ^2} \left\{ (1 - \xi^2) |\langle \tilde{H} \rangle|^2 - 2\xi^2 \Re \left[\langle \tilde{H} \rangle^* \langle \tilde{E} \rangle \right] - \frac{t'}{4m^2} \xi^2 |\langle \tilde{E} \rangle|^2 \right\} \quad (1.24)$$

$$\frac{d\sigma_T}{dt} = \frac{2\pi\alpha\mu_\pi^2}{kQ^4} \left\{ (1 - \xi^2) |\langle H_T \rangle|^2 - \frac{t'}{8m^2} |\langle \bar{E}_T \rangle|^2 \right\} \quad (1.25)$$

$$\frac{d\sigma_{LT}}{dt} = \frac{4\pi\alpha\mu_\pi}{\sqrt{2}kQ^3} \xi \sqrt{1 - \xi^2} \frac{\sqrt{-t'}}{2m} \Re \left\{ \langle H_T \rangle^* \langle \tilde{E} \rangle \right\} \quad (1.26)$$

$$\frac{d\sigma_{TT}}{dt} = \frac{4\pi\alpha\mu_\pi^2}{kQ^4} \frac{-t'}{16m^2} \langle \bar{E}_T \rangle^2 \quad (1.27)$$

The terms involved in these expressions are:

- $t' = t - t_0$ where $t_0 = \frac{-4m^2\xi^2}{1-\xi^2}$
- Skewness $\xi = \frac{x_B}{2-x_B}$
- The bracket $\langle \tilde{F} \rangle$ is the convolution of a GPD and an appropriate subprocess amplitude: $\langle \tilde{F} \rangle = \sum_\lambda \int_{-1}^1 d\bar{x} H_{0\lambda,0\lambda}(\bar{x}, \xi, Q^2, t=0) \tilde{F}(\bar{x}, \xi, Q^2, t)$
 - λ is the unobserved helicities of the partons participating in the subprocess
- Phase space factor $k = 16\pi \left(W^2 - m^2 \right) \sqrt{\Lambda(W^2, -Q^2, m^2)}$
 - $\Lambda(W^2, -Q^2, m^2)$ is the Källén function: $W^4 + Q^4 + m^4 + 2W^2Q^2 + 2Q^2m^2 - 2W^2m^2$
- Reduced pion mass $\mu_{\pi^0} = \frac{m_{\pi^0}^2}{m_u + m_d}$
 - m_u and m_d are respective masses of up and down quarks

1.2.3 Status of DV π^0 P Measurements

With theoretical advancements occurring in the mid 1990s to early 2000s, the first analyses of experimental measurements of DV π^0 P have only been released in the past decade.

Summary of Existing Measurements

The earliest of such measurements were taken at the Thomas Jefferson National Accelerator Facility (JLab) with a ~ 6 GeV electron beam. Two of the four experimental halls - Hall A ([Fuchey et al., 2011](#)) and Hall B ([Bedlinskiy et al., 2014](#)) produced cross-section results. Hall A houses a small acceptance precision spectrometer and recorded data in several kinematic bins. Hall B housed a large acceptance spectrometer, yielding cross-section measurements over a large kinematic regime.

Recent upgrades at JLab have nearly doubled the beam energy to 10.6 GeV, and both detector halls have accumulated data allowing for the measurement of this process. Both halls repeated data taking at this higher energy, with Hall A recently releasing updated cross-section values across three fixed x_B bins (0.36, 0.48 and 0.6) and over a range of Q^2 values from 3 to 9 GeV 2 ([Dlamini et al., 2021](#)).

This work expands on these results by covering a much larger kinematic regime, as well as having much higher statistics compared to the 6 GeV Hall B result. A kinematic overlap plot in Q^2 , x_B is shown in Fig. [1-16](#) summarizes these differences. It is also noted that the CERN COMPASS collaboration ([Alexeev et al., 2020](#)) has measured this process using a 160 GeV muon beam, obtaining results over a much lower x_B range.

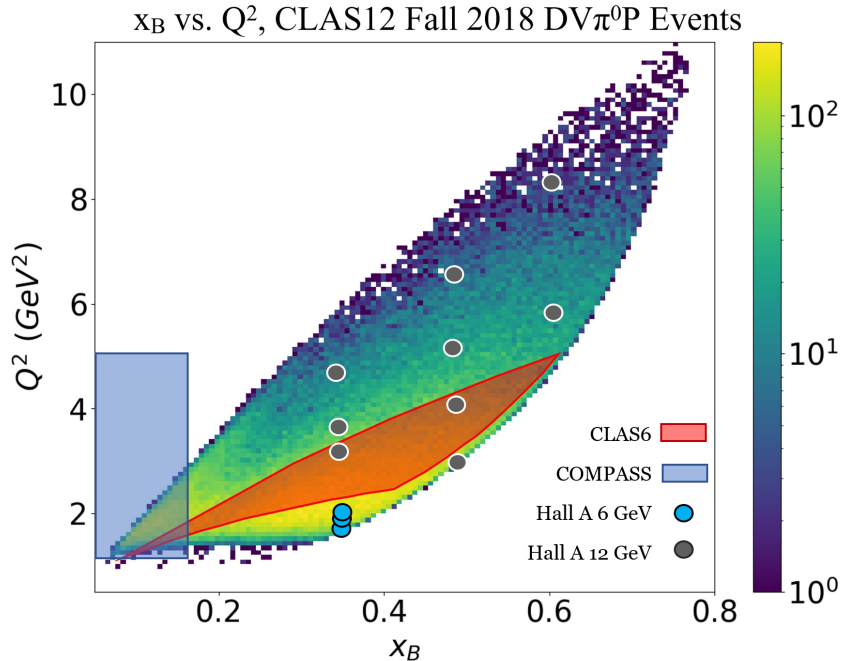


Figure 1-16: Kinematic reach plot between this work and other results: CLAS6 ([Bedlinskiy et al., 2014](#)), COMPASSS ([Alexeev et al., 2020](#)), Hall A 6 GeV ([Fuchey et al., 2011](#)), and Hall A 12 GeV ([Dlamini et al., 2021](#)). The reach shown for Hall A are approximate areas around their reported bin centers.

Overview of This Measurement

This work details the analysis of data taken at the JLab CLAS12 experiment to measure the deeply virtual neutral pion electroproduction cross-section . Chapter ?? describes the experimental setup. Chapter ?? discusses the computational and simulational infrastructure built and used as an integral part in estimating correction factors and performing an accurate measurement. Chapter ?? explains the specific analysis procedures and estimation methods used to arrive at cross-section values. Chapter ?? presents further physics analysis, made possible with the extracted cross-

section values. Fig. 1-17 broadly summarizes the analysis flow; electronic readers can conveniently click on boxes for hyperlinks to relevant sections.

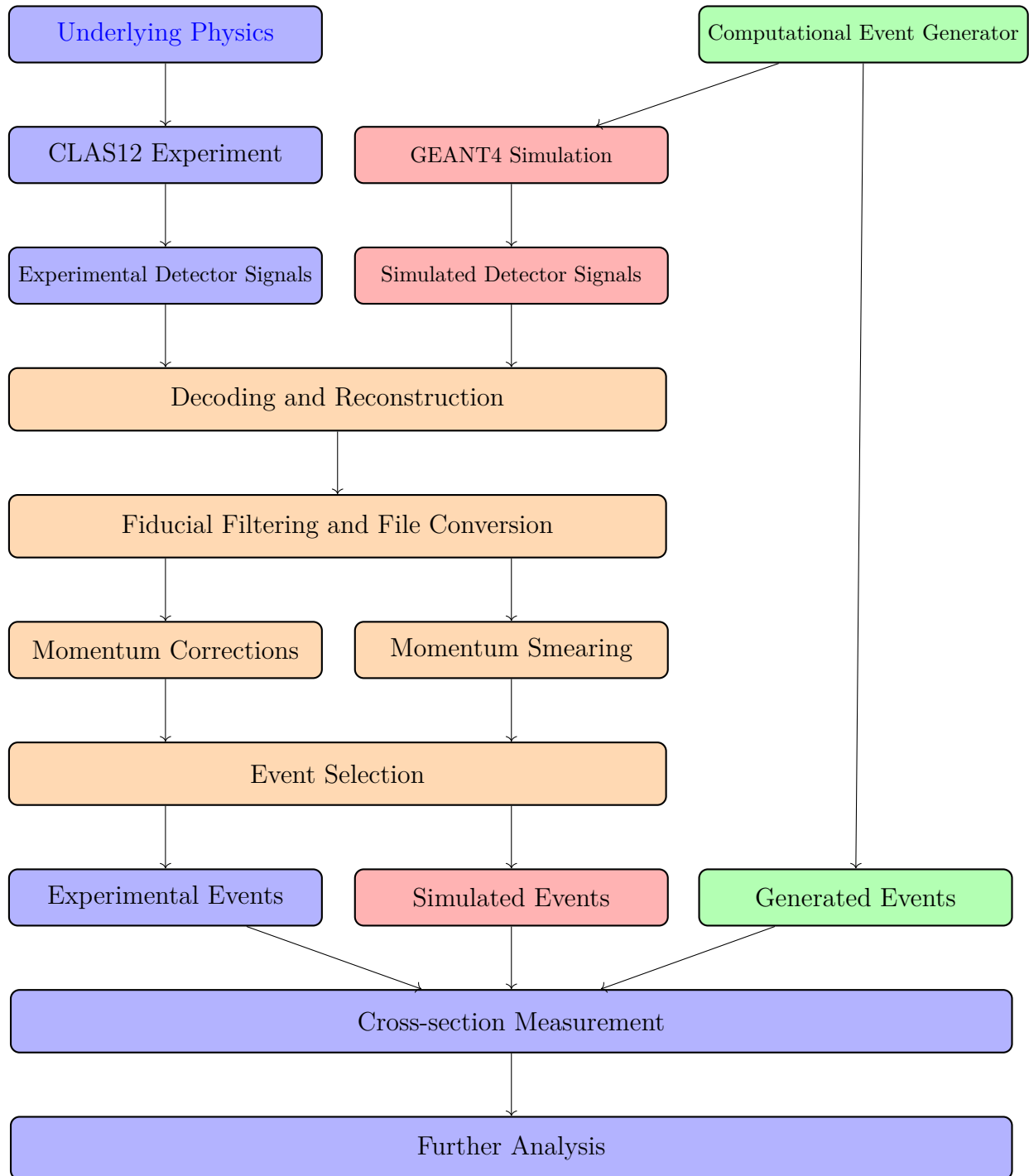


Figure 1-17: Analysis Overview Flowchart

Bibliography

- [1] M.G. Alexeev et al. “Measurement of the cross section for hard exclusive $\pi 0$ muoproduction on the proton”. In: *Physics Letters B* 805 (June 2020), p. 135454. ISSN: 03702693. DOI: [10.1016/j.physletb.2020.135454](https://doi.org/10.1016/j.physletb.2020.135454). URL: <https://www.sciencedirect.com/science/article/pii/S0370269320302586/pdf> (cit. on pp. 40, 41).
- [2] G. Altarelli and G. Parisi. “Asymptotic freedom in parton language”. In: *Nuclear Physics B* 126.2 (Aug. 1977), pp. 298–318. ISSN: 05503213. DOI: [10.1016/0550-3213\(77\)90384-4](https://doi.org/10.1016/0550-3213(77)90384-4). URL: <https://www.sciencedirect.com/science/article/pii/0550321377903844> (cit. on p. 24).
- [3] E. Amaldi, S. Fubini, and G. Furlan. *Pion-electroproduction*. Vol. 83. Berlin, Heidelberg: Springer Berlin Heidelberg, 1979, pp. 1–10. ISBN: 978-3-540-08998-8. DOI: [10.1007/BFb0048208](https://doi.org/10.1007/BFb0048208) (cit. on pp. 37, 38).
- [4] I. Bedlinskiy et al. “Exclusive Neutral Pion electroproduction at $W > 2$ GeV with CLAS”. In: *Physical Review C - Nuclear Physics* 90.2 (2014). ISSN: 1089490X. DOI: [10.1103/PhysRevC.90.025205](https://doi.org/10.1103/PhysRevC.90.025205). URL: <https://journals.aps.org/prc/abstract/10.1103/PhysRevC.90.025205%20https://arxiv.org/pdf/1405.0988.pdf> (cit. on pp. 37, 40, 41).

- [5] J. D. Bjorken and E. A. Paschos. “Inelastic Electron-Proton and gamma-Proton Scattering and the Structure of the Nucleon”. In: *Physical Review* 185.5 (Sept. 1969), pp. 1975–1982. ISSN: 0031-899X. DOI: [10.1103/PhysRev.185.1975](https://doi.org/10.1103/PhysRev.185.1975). URL: <https://journals.aps.org/pr/abstract/10.1103/PhysRev.185.1975> (cit. on p. 22).
- [6] The Editors of Encyclopaedia Britannica. *law of multiple proportions*. 2010. URL: <https://www.britannica.com/science/law-of-multiple-proportions> (cit. on p. 11).
- [7] The Editors of Encyclopaedia Britannica. *Thomson atomic model*. 2023. URL: <https://www.britannica.com/science/Thomson-atomic-model> (cit. on p. 12).
- [8] Louis de Broglie. “A tentative theory of light quanta”. In: *The London, Edinburgh, and Dublin Philosophical Magazine and Journal of Science* 47.278 (Feb. 1924), pp. 446–458. ISSN: 1941-5982. DOI: [10.1080/14786442408634378](https://doi.org/10.1080/14786442408634378). URL: <https://www.tandfonline.com/doi/full/10.1080/14786442408634378?scroll=top&needAccess=true&role=tab> (cit. on p. 14).
- [9] M. Burkardt and B. Pasquini. “Modelling the nucleon structure”. In: *The European Physical Journal A* 52.6 (June 2016), p. 161. ISSN: 1434-6001. DOI: [10.1140/epja/i2016-16161-7](https://doi.org/10.1140/epja/i2016-16161-7). URL: <https://arxiv.org/pdf/1510.02567.pdf> (cit. on p. 30).
- [10] Matthias Burkardt. “GPDs with ζ Not Equal to 0”. In: *ArXiv* (Nov. 2007). URL: <https://arxiv.org/pdf/0711.1881.pdf> (cit. on pp. 30, 36).
- [11] V. D. Burkert, L. Elouadrhiri, and F. X. Girod. “The pressure distribution inside the proton”. In: *Nature* 557.7705 (May 2018), pp. 396–399. ISSN: 0028-

0836. DOI: [10.1038/s41586-018-0060-z](https://doi.org/10.1038/s41586-018-0060-z). URL: <https://www.nature.com/articles/s41586-018-0060-z> (cit. on p. 32).

- [12] C.C.W. Taylor. *The atomists, Leucippus and Democritus: fragments, a text and translation with a commentary*. University of Toronto Press, 1999, pp. 157–158. ISBN: 0-8020-4390-9 (cit. on p. 11).
- [13] J. Chadwick. “Possible Existence of a Neutron”. In: *Nature* 129.3252 (Feb. 1932), pp. 312–312. ISSN: 0028-0836. DOI: [10.1038/129312a0](https://doi.org/10.1038/129312a0) (cit. on p. 13).
- [14] Fei Chen, Paul W. Tillberg, and Edward S. Boyden. “Expansion microscopy”. In: *Science* 347.6221 (Jan. 2015), pp. 543–548. ISSN: 0036-8075. DOI: [10.1126/science.1260088](https://doi.org/10.1126/science.1260088). URL: <https://www.science.org/doi/10.1126/science.1260088> (cit. on p. 14).
- [15] S. Diehl et al. “Extraction of Beam-Spin Asymmetries from the Hard Exclusive π^+ Channel off Protons in a Wide Range of Kinematics”. In: *Physical Review Letters* 125.18 (Oct. 2020), p. 182001. ISSN: 0031-9007. DOI: [10.1103/PhysRevLett.125.182001](https://doi.org/10.1103/PhysRevLett.125.182001). URL: <https://journals.aps.org/prl/abstract/10.1103/PhysRevLett.125.182001%20https://arxiv.org/pdf/2007.15677.pdf> (cit. on p. 36).
- [16] M. Dlamini et al. “Deep Exclusive Electroproduction of $\pi^+ \rightarrow \pi^+ Q^-$ at High Q^2 in the Quark Valence Regime”. In: *Physical Review Letters* 127.15 (Oct. 2021), p. 152301. ISSN: 0031-9007. DOI: [10.1103/PhysRevLett.127.152301](https://doi.org/10.1103/PhysRevLett.127.152301). URL: <https://journals.aps.org/prl/pdf/10.1103/PhysRevLett.127.152301> (cit. on pp. 40, 41).

- [17] A. Donnachie and G. Shaw. “Generalized Vector Dominance”. In: *Electromagnetic Interactions of Hadrons*. Boston, MA: Springer US, 1978, pp. 169–194. DOI: [10.1007/978-1-4757-0713-7__3](https://doi.org/10.1007/978-1-4757-0713-7_3) (cit. on p. 37).
- [18] T. William Donnelly et al. *Foundations of Nuclear and Particle Physics*. Cambridge University Press, Feb. 2017. ISBN: 9780521765114. DOI: [10.1017/9781139028264](https://doi.org/10.1017/9781139028264) (cit. on p. 21).
- [19] T.W. Donnelly, Sabine Jeschonnek, and J.W. Van Orden. “General tensor structure for electron scattering in terms of invariant responses”. In: *Annals of Physics* 448 (Jan. 2023), p. 169174. ISSN: 00034916. DOI: [10.1016/j.aop.2022.169174](https://doi.org/10.1016/j.aop.2022.169174) (cit. on p. 37).
- [20] D Dreschsel and L Tiator. “Threshold pion photoproduction on nucleons”. In: *Journal of Physics G: Nuclear and Particle Physics* 18.3 (Mar. 1992), pp. 449–497. ISSN: 0954-3899. DOI: [10.1088/0954-3899/18/3/004](https://doi.org/10.1088/0954-3899/18/3/004). URL: <https://iopscience.iop.org/article/10.1088/0954-3899/18/3/004/pdf> (cit. on p. 36).
- [21] Richard P. Feynman. “Very High-Energy Collisions of Hadrons”. In: *Physical Review Letters* 23.24 (Dec. 1969), pp. 1415–1417. ISSN: 0031-9007. DOI: [10.1103/PhysRevLett.23.1415](https://doi.org/10.1103/PhysRevLett.23.1415). URL: <https://journals.aps.org/prl/abstract/10.1103/PhysRevLett.23.1415%20https://authors.library.caltech.edu/3871/1/FEYprl69.pdf> (cit. on p. 23).
- [22] Linda E. Franken et al. “A Technical Introduction to Transmission Electron Microscopy for Soft-Matter: Imaging, Possibilities, Choices, and Technical Developments”. In: *Small* 16.14 (Apr. 2020), p. 1906198. ISSN: 1613-6810. DOI: [10.1002/smll.201906198](https://doi.org/10.1002/smll.201906198). URL: <https://onlinelibrary.wiley.com/doi/full/10.1002/smll.201906198> (cit. on p. 14).

- [23] E. Fuchey et al. “Exclusive neutral pion electroproduction in the deeply virtual regime”. In: *Physical Review C* 83.2 (Feb. 2011), p. 025201. ISSN: 0556-2813. DOI: [10.1103/PhysRevC.83.025201](https://doi.org/10.1103/PhysRevC.83.025201). URL: <https://journals.aps.org/prc/abstract/10.1103/PhysRevC.83.025201>%20<https://arxiv.org/pdf/1003.2938.pdf> (cit. on pp. 40, 41).
- [24] Hans Geiger and Ernest Marsden. “On a Diffuse Reflection of the alpha-Particles”. In: *Proceedings of the Royal Society of London Series A* 82.557 (1909), pp. 495–500 (cit. on p. 13).
- [25] S. V. Goloskokov and P. Kroll. “An attempt to understand exclusive π^+ electroproduction”. In: *The European Physical Journal C* 65.1-2 (Jan. 2010), p. 137. ISSN: 1434-6044. DOI: [10.1140/epjc/s10052-009-1178-9](https://doi.org/10.1140/epjc/s10052-009-1178-9). URL: <https://link.springer.com/content/pdf/10.1140/epjc/s10052-009-1178-9.pdf> (cit. on p. 30).
- [26] M. Hillery et al. “Distribution functions in physics: Fundamentals”. In: *Physics Reports* 106.3 (Apr. 1984), pp. 121–167. ISSN: 03701573. DOI: [10.1016/0370-1573\(84\)90160-1](https://doi.org/10.1016/0370-1573(84)90160-1). URL: <http://ursula.chem.yale.edu/~batista/classes/v572/Scully.pdf> (cit. on p. 28).
- [27] Jaume Navarro. *A History of the Electron: J.J. and G.P. Thomson*. Cambridge University Press, 1995. ISBN: 978-1-107-00522-8. (Cit. on p. 12).
- [28] Xiangdong Ji. “Gauge-Invariant Decomposition of Nucleon Spin”. In: *Physical Review Letters* 78.4 (Jan. 1997), pp. 610–613. ISSN: 0031-9007. DOI: [10.1103/PhysRevLett.78.610](https://doi.org/10.1103/PhysRevLett.78.610). URL: <https://journals.aps.org/prl/abstract/10.1103/PhysRevLett.78.610>%20<https://arxiv.org/pdf/hep-ph/9603249.pdf> (cit. on p. 30).

- [29] Xiangdong Ji. “GENERALIZED PARTON DISTRIBUTIONS”. In: *Annual Review of Nuclear and Particle Science* 54.1 (Dec. 2004), pp. 413–450. ISSN: 0163-8998. DOI: [10.1146/annurev.nucl.54.070103.181302](https://doi.org/10.1146/annurev.nucl.54.070103.181302). URL: <https://www.annualreviews.org/doi/10.1146/annurev.nucl.54.070103.181302> (cit. on pp. 28, 29).
- [30] Max Klein. *Resolving the Inner Structure of Matter The H1 Experiment at HERA*. Tech. rep. Workshop at Podgorica - 25 years of the Science Faculty, 2005 (cit. on p. 26).
- [31] Valery Kubarovsky. “Deeply Virtual Exclusive Reactions with CLAS”. In: *Nuclear Physics B - Proceedings Supplements* 219-220 (Oct. 2011), pp. 118–125. ISSN: 09205632. DOI: [10.1016/j.nuclphysbps.2011.10.080](https://doi.org/10.1016/j.nuclphysbps.2011.10.080). URL: <https://www.sciencedirect.com/science/article/pii/S0920563211008218/pdf?md5=2efd6bc3a69acdce62fc3d0bfa1be5c5&pid=1-s2.0-S0920563211008218-main.pdf> (cit. on p. 32).
- [32] Xuezhi Ma et al. “6 nm super-resolution optical transmission and scattering spectroscopic imaging of carbon nanotubes using a nanometer-scale white light source”. In: *Nature Communications* 12.1 (Nov. 2021), p. 6868. ISSN: 2041-1723. DOI: [10.1038/s41467-021-27216-5](https://doi.org/10.1038/s41467-021-27216-5) (cit. on p. 14).
- [33] Ernest Rutherford. “Collision of alpha Particles with Light Atoms. IV. An Anomalous Effect in Nitrogen”. In: *Philosophical Magazine Series 6* 37 (1919), pp. 581–587. URL: <https://www.tandfonline.com/doi/abs/10.1080/14786431003659230> (cit. on p. 13).
- [34] Ernest Rutherford. “The Scattering of Alpha and Beta Particles by Matter and the Structure of the Atom”. In: *Philosophical Magazine Series 6* 21 (1911), pp. 669–688 (cit. on p. 13).

- [35] P. E. Shanahan and W. Detmold. “Pressure Distribution and Shear Forces inside the Proton”. In: *Physical Review Letters* 122.7 (Feb. 2019), p. 072003. ISSN: 0031-9007. DOI: [10.1103/PhysRevLett.122.072003](https://doi.org/10.1103/PhysRevLett.122.072003). URL: <https://journals.aps.org/prl/abstract/10.1103/PhysRevLett.122.072003> 20<https://arxiv.org/pdf/1810.07589.pdf> (cit. on p. 32).
- [36] Thomas McEvilley. *The Shape of Ancient Thought: Comparative Studies in Greek and Indian Philosophies*. New York: Allworth Press, 2002. ISBN: 978-0-8020-4390-0 (cit. on p. 11).
- [37] J.J. Thomson. “On Bodies Smaller than Atoms”. In: *The Popular Science Monthly* (1901), pp. 323–325. URL: <https://books.google.com/books?id=3CMDAAAAMBAJ&pg=PA323#v=onepage&q&f=false> (cit. on p. 11).
- [38] Mark Thomson. *Modern Particle Physics*. Cambridge University Press, Sept. 2013, pp. 160–204. ISBN: 9781107034266. DOI: [10.1017/CBO9781139525367](https://doi.org/10.1017/CBO9781139525367) (cit. on pp. 19, 22).
- [39] E. Wigner. “On the Quantum Correction For Thermodynamic Equilibrium”. In: *Physical Review* 40.5 (June 1932), pp. 749–759. ISSN: 0031-899X. DOI: [10.1103/PhysRev.40.749](https://doi.org/10.1103/PhysRev.40.749). URL: https://lab409.chem.ccu.edu.tw/~yach932/CH3_Reference/51.PhysRev.40.749.pdf (cit. on p. 27).
- [40] David B. Williams and C. Barry Carter. *Transmission Electron Microscopy*. Boston, MA: Springer US, 2009. ISBN: 978-0-387-76500-6. DOI: [10.1007/978-0-387-76501-3](https://doi.org/10.1007/978-0-387-76501-3). URL: <https://link.springer.com/book/10.1007/978-0-387-76501-3> (cit. on pp. 14, 15).
- [41] P A Zyla et al. “Review of Particle Physics”. In: *Progress of Theoretical and Experimental Physics* 2020.8 (Aug. 2020). ISSN: 2050-3911. DOI: [10.1093/ptep/ptaa08](https://doi.org/10.1093/ptep/ptaa08)

ptep/ptaa104. URL: <https://pdg.lbl.gov/2020/reviews/rpp2020-rev-structure-functions.pdf> (cit. on pp. 24, 25).

Appendix A

Full Cross Section Data

To be completed

Appendix B

BSA Cross Check

As an additional cross check, Bobby calculated a $DV\pi^0P$ beam spin asymmetry and compared to Andrey Kim's results. This check will not comment on any acceptance, luminosity, or virtual photon flux factor calculations, but does validate exclusive event selection criteria. By examining figure [B-1](#) we can see that agreement is reasonable, especially considering Bobby's calculation does not have sideband subtraction included.

Fig [B-1](#) shows an overlay comparison of Andrey Kim's results (black datapoints, red fit line) and Bobby's results (red datapoints, orange fit line)

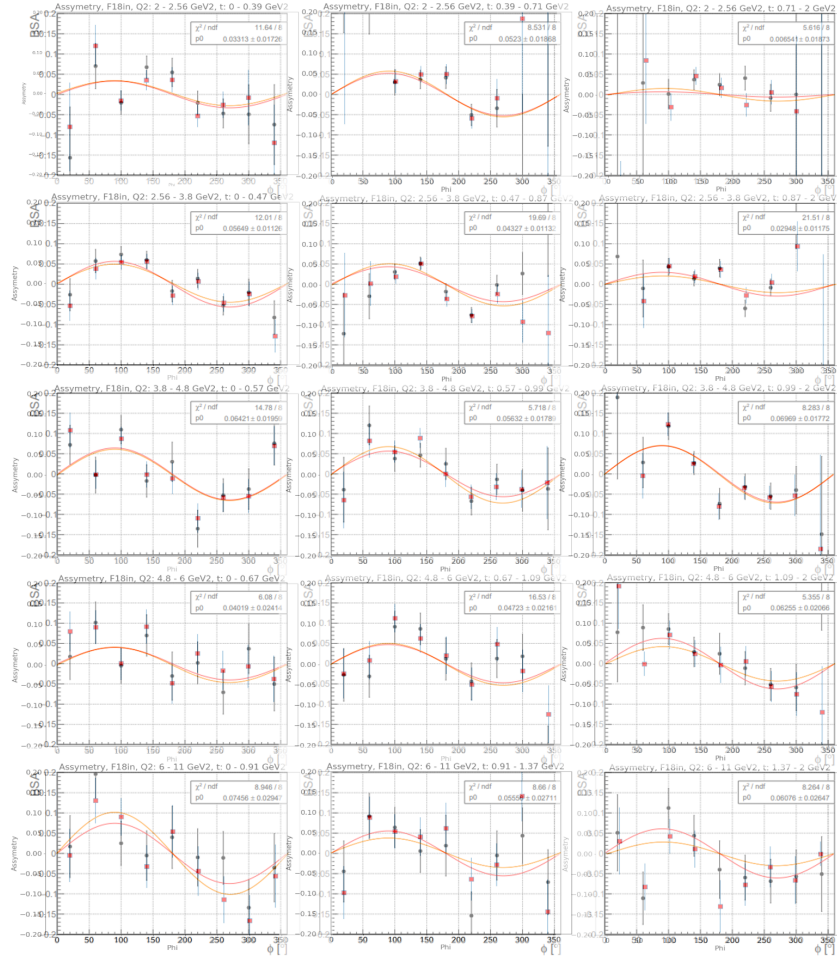


Figure B-1: BSA Cross Check Results

Appendix C

Derivation of phi math convention

Thus: $\phi = \arccos((\mathbf{v3l} \cdot \mathbf{v3h}) / (\text{mag } \mathbf{v3l} \text{ mag } \mathbf{v3h}))$

$$\phi = \cos^{-1} \left(\frac{(\mathbf{p}_e \times \mathbf{p}_{e'}) \cdot (\mathbf{p}_{p'} \times \mathbf{p}_{\gamma^*})}{\|\mathbf{p}_e \times \mathbf{p}_{e'}\| \|\mathbf{p}_{p'} \times \mathbf{p}_{\gamma^*}\|} \right)$$

if $\text{dot}(\mathbf{p}_e \times \mathbf{p}_{e'}, \mathbf{p}_{p'})$ is greater than 0, then do $360 - \phi = \phi$. If we expand the above out, we get: $-\mathbf{p}_{p'} \cdot \mathbf{e}_z \mathbf{e}_y + \mathbf{p}_y \cdot \mathbf{e}_z \mathbf{e}_x$ is greater than zero which we can reduce to $-\mathbf{p}_{p'} \cdot \mathbf{e}_y + \mathbf{p}_y \cdot \mathbf{e}_x$ is greater than zero

By inspecting table below, we can see what this really amounts to, is the trento convention saying that we take the angle by measuring counterclockwise from the proton vector to the electron vector.

$360 - \theta$ when $|p'_x e'_x| > |p'_x e'_y|$

p'_y	p'_x	e'_y	e'_x	L	R	θ	$ p'_x > e'_x $	$ p'_x < e'_x $
-	-	-	-	+	+		-	-
-	-	-	+	-	+	$< 180^\circ$	-	+
-	-	t	-	+	-	$> 180^\circ$		+
-	-	+	+	-	-		$> 180^\circ$	
-	+	-	-	+	-			
-	+	-	+	-	+			
-	+	+	+	-	+			
-	+	+	+	+	+			

$-e'_x > -e'_y$ $e'_x < e'_y$ $|e'_x| > |e'_y|$ shows m

